

Reconfigurable exceptional point-based sensing with 0.001λ sensitivity using spoof localized surface plasmons

Yaoran Zhang,^{a,†} Hao Hu,^{a,†} Francisco José García-Vidal,^b Jingjing Zhang,^c Liangliang Liu^{id},^{a,*} Yu Luo^{id},^{a,d,*} and Zhuo Li^{id},^{a,*}

^aNanjing University of Aeronautics and Astronautics, College of Electronic and Information Engineering, National Key Laboratory of Microwave Photonics, Nanjing, China

^bUniversidad Autónoma de Madrid, Departamento de Física Teórica de la Materia Condensada and Condensed Matter Physics Center, Madrid, Spain

^cSoutheast University, State Key Laboratory of Millimeter Waves, Nanjing, China

^dNanyang Technological University, School of Electrical and Electronic Engineering, Singapore

Abstract. Recent breakthroughs in the field of non-Hermitian physics present unprecedented opportunities, from fundamental theories to cutting-edge applications such as multimode lasers, unconventional wave transport, and high-performance sensors. The exceptional point, a spectral singularity widely existing in non-Hermitian systems, provides an indispensable route to enhance the sensitivity of optical detection. However, the exceptional point of the forementioned systems is set once the system is built or fabricated, and machining errors make it hard to reach such a state precisely. To this end, we develop a highly tunable and reconfigurable exceptional point system, i.e., a single spoof plasmonic resonator suspended above a substrate and coupled with two freestanding Rayleigh scatterers. Our design offers great flexibility to control exceptional point states, enabling us to dynamically reconfigure the exceptional point formed by various multipolar modes across a broadband frequency range. Specifically, we experimentally implement five distinct exceptional points by precisely manipulating the positions of two movable Rayleigh scatterers. In addition, the enhanced perturbation strength offers remarkable sensitivity enhancement for detecting deep-subwavelength particles with the minimum dimension down to 0.001λ (with λ to be the free-space wavelength).

Keywords: non-Hermitian optics; spoof localized surface plasmons; exceptional points; ultrasensitive microwave sensors.

Received Jun. 26, 2024; accepted for publication Jul. 18, 2024; published online Aug. 20, 2024.

© The Authors. Published by SPIE and CLP under a Creative Commons Attribution 4.0 International License. Distribution or reproduction of this work in whole or in part requires full attribution of the original publication, including its DOI.

[DOI: [10.1117/1.APN.3.5.056004](https://doi.org/10.1117/1.APN.3.5.056004)]

1 Introduction

In the past two decades, exceptional point (EP) has had a far-reaching impact in various research fields ranging from quantum mechanics and acoustics to photonics. EP corresponds to a spectral singularity in the parameter space of a non-Hermitian system where at least two eigenvalues and their associated eigenfunctions simultaneously coalesce.^{1–3} Such peculiar degeneracies give rise to a wealth of novel effects, such as parity-

time phase transition, topological phase transition,^{4,5} and self-intersecting Riemann surface.⁶ These exotic phenomena not only enrich non-Hermitian physics but also lead to many practical applications including coherent-perfect absorption,^{7,8} EP sensing,⁹ nonreciprocal wave propagation,^{10,11} reconfigurable topological lasers,¹² and more.^{13,14}

For EP sensing applications, the whispering gallery mode (WGM) microtoroid has long been regarded as one of the most promising platforms.^{15–20} In the presence of target particles, the induced perturbation leads to the splitting of resonant frequencies that are initially degenerated at the EP.²¹ As such, measuring the amount of frequency splitting enables us to acquire information about particle sizes. Remarkably, the WGM microtoroid

*Address all correspondence to Liangliang Liu, lliu@nuaa.edu.cn; Yu Luo, yu.luo@nuaa.edu.cn; Zhuo Li, lizhuo@nuaa.edu.cn

[†]These authors contributed equally to this work.

operating at or close to EPs has been revealed to exhibit three-²² to seven-fold²³ higher sensitivity as compared to that of conventional sensors, e.g., the WGM microtoroid operating near diabolic points (DPs) where only the system eigenvalues coalesce.

To widen the detectable range of particle dimensions, extending the working bandwidth of EP sensors is highly desirable. Nevertheless, EP sensors based on WGM microtoroid generally work at a particular order of WGM, i.e., a single frequency, due to the following two constraints.²⁴ On the one hand, optical fields mainly concentrate inside the microtoroid, limiting the perturbation strength induced by external target particles. This limitation further hinders the above EP sensors in detecting subwavelength particles (with the minimum reported detectable size down to 0.258λ). In other words, such sensors must work at a sufficiently higher-order (or higher-frequency) mode to detect a particle in a given dimension. On the other hand, as the mode order (or frequency) further increases,²⁵ the enhanced Q -factor dramatically lowers the excitation efficiency of WGM. In this case, the optical response of the sensor is too weak to detect the target particles. Thus, although a reconfigurable EP sensor (i.e., the one with tunable EPs) has long been sought after, its realization still confronts scientific challenges.

Spoof plasmonic resonators, e.g., spoof localized surface plasmon (LSP) resonators, emerge as an alternative platform for EP sensing.²⁶⁻³¹ A spoof LSP resonator refers to a periodically textured closed metallic structure that supports WGM-like modes (i.e., spoof LSPs) in multiple resonance frequencies.³²⁻³⁸ Recently, an electrically controllable EP within a spoof LSP structure was first reported in the microwave domain, which is realized by perturbing plasmonic modes with an angled metal line and a varactor.³⁸ Moreover, Zhang et al. proposed an EP sensor based on a chiral microwave spoof LSP resonator working at the fundamental dipole mode.³⁹ Despite their similarity to WGMs in the spectrum, spoof LSPs are strongly localized at the surface or edge of resonators rather than within the bulk, which is a key merit that facilitates the realization of reconfigurable EP sensors.

First of all, the strong field confinement at the structural surface/edge largely enhances the perturbation strength from the surrounding target particles. The enhanced perturbation strength allows the detection of particles in the subwavelength scale (with the size down to 0.004λ ³⁹ and 0.012λ ,⁴⁰ as reported by recent experimental works). This also means that lower-order (i.e., lower-frequency) modes in the platform of spoof plasmonic resonators are now feasible to create EP,³⁹ which is, however, unavailable in the platform of WGM resonators. Moreover, surface field enhancement also largely improves the excitation efficiency of multipolar modes, opening up an opportunity to form EP with high-order modes. Although recent advances³⁸⁻⁴¹ demonstrate the superior sensitivity of EP sensors constructed by spoof plasmonic resonators, the EP state is fixed and cannot be adjusted once the spoof plasmonic resonator is fabricated, indicating that the proposed schemes lack the degree of freedom to tune the EPs. In addition, the aforementioned scheme may fail to work at the EP state due to a tiny fabrication error. Therefore, although spoof plasmonic resonators offer a feasible solution to construct EP sensors, their realization of tunable and reconfigurable EP sensors remains unexplored.

To this end, we experimentally demonstrate reconfigurable and tunable EP sensors in the platform of spoof plasmonic resonators. The configuration consists of a spoof plasmonic resonator, a microstrip line, and two movable Rayleigh scatterers.

Different from the conventional structural setup, the spoof plasmonic resonator is intentionally suspended above the microstrip line via an individual metal disk. We note that such a wise design has three main advantages. First, it leaves a sufficiently large space to tune the system to the EP state by adjusting the two Rayleigh scatterers. Second, it greatly improves the excitation efficiency of multipolar spoof LSPs. Third, it further enhances the perturbation strength of target particles. In addition, the mobility of Rayleigh scatterers offers a great degree of freedom to flexibly switch the EPs at distinct resonance mode in a broad range of frequencies. As we will show later, our experimental results successfully realize five consecutive EPs from sextupole, octupole, decapole, and dodecapole to 14-pole resonance modes. Owing to the extraordinarily strong perturbation strength, the proposed EP reconfigurable sensor exhibits superior sensitivity, with the minimum detectable dimension down to 0.001λ . Such a value is even a quarter magnitude of the recently reported result.³⁹ Our work thus provides a novel paradigm for realizing flexible and highly sensitive particle detection from microwave to terahertz frequencies.

2 Materials and Methods

2.1 Principles of the EP Sensor

The schematic of the designed reconfigurable EP sensing system is shown in Fig. 1. The sensing system involves a single spoof plasmonic resonator suspended on the substrate and a

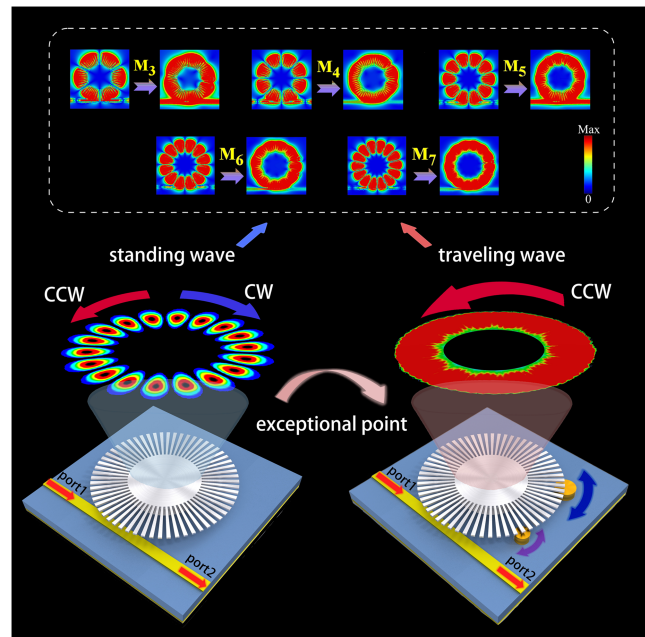


Fig. 1 Schematic illustration of the tunable and reconfigurable EP sensing system on a single plasmonic resonator. The bottom half shows the DP sensor in the absence of particles and the second-order EP sensor with two dynamically movable Rayleigh scatterers. One essential characteristic of the EP is the emergence of a unidirectional propagation traveling wave on the plasmonic resonator. The top half demonstrates the z -component of the electric field E_z from standing wave (DP sensor) to traveling wave (EP sensor) of the reconfigurable EPs in five consecutive plasmonic resonance modes.

microstrip line underneath. As the nature of spoof plasmonic structures, the resonator exhibits analogous characteristics to optical WGM cavities with multimode resonances, where each mode supports clockwise (CW) and counterclockwise (CCW) propagating waves with degenerate eigenfrequencies but orthogonal eigenvectors. In the absence of external perturbation, the proposed spoof plasmonic resonator operating at a DP supports equivalent magnitudes of CW and CCW propagating waves, thus spatially reflected as a standing-wave mode (see mode distribution in the bottom left of Fig. 1). When a single scatterer is placed close to the spoof plasmonic resonator, the scatterer will perturb the WGMs via the evanescent coupling. As a result, the coherent backscattering of counterpropagating waves will lift the spectral degeneracy with a doublet of standing-wave modes. Interestingly, when another scatterer with a proper size is introduced into this open system at a specific position, non-Hermitian degeneracy known as the second-order EP emerges, where eigenfrequencies and their corresponding eigenvectors coalesce simultaneously. Under this circumstance, the EP sensor displays fully asymmetric backscattering between the CW and CCW propagating waves, and only one of the traveling directions is dominant, as depicted in the bottom right of Fig. 1. Note that the above differences between spoof plasmonic resonators with and without EP apply to all the multipolar modes (see corresponding comparison of field distributions at the top of Fig. 1, and the phase distributions are illustrated in Sec. S1 in the [Supplementary Material](#)), further validating the implementation of reconfigurable EPs in five consecutive plasmonic resonance modes.

To demonstrate the advantage of the EP sensor, we theoretically compare its sensitivity with the DP sensor. In the DP sensor, the magnitude of frequency splitting is directly proportional to the perturbation strength, denoted as ε . However, for the resonator operating at second-order EPs, the splitting induced by the identical perturbation is proportional to $\varepsilon^{1/2}$. Consequently, when encountering sufficiently small target particles, the EP sensor shows larger frequency splitting, which can be described as^{16,22,24}

$$\Delta\omega_{\text{EP}} = \Delta\omega_{\text{DP}} \sqrt{1 + \frac{A_j^{(2)}}{\varepsilon} e^{i2m_j\alpha}}, \quad (1)$$

where $\Delta\omega_{\text{DP}} = 2 \cdot \varepsilon \cdot m_j$ denotes the mode number of plasmonic mode j and $A_j^{(2)}$ represents the unidirectional backscattering generated by second-order EPs. The perturbation strength of the target particle is $\varepsilon = \varepsilon_3$ and the relative azimuthal angle is $\alpha = \alpha_3$. In the case of $|A_j^{(2)}| \gg |\varepsilon|$, Eq. (1) can be simplified to

$$\Delta\omega_{\text{EP}} = \Delta\omega_{\text{DP}} \sqrt{\frac{A_j^{(2)}}{\varepsilon} e^{i2m_j\alpha}} = 2\sqrt{A_j^{(2)}\varepsilon} e^{im_j\alpha}. \quad (2)$$

Hence, the frequency splitting of EP sensors is proportional to $\varepsilon^{1/2}$, indicating a reinforced capacity for detecting sufficiently small target particles. Thus, the spoof plasmonic sensor exhibits significantly enhanced sensitivity to external perturbations when operating at EPs. In addition, the sensitivity enhancement $|\Delta\omega_{\text{EP}}/\Delta\omega_{\text{DP}}|$ is directly proportional to the square root of $|A_j^{(2)}|$ but inversely proportional to $\sqrt{|\varepsilon|}$ (see Sec. S2 in the [Supplementary Material](#)).

2.2 Structural Design of the Reconfigurable EP Sensor

The proposed EP sensor is schematically illustrated in Figs. 2(a)–2(c), including the suspended spoof plasmonic resonator instead of the directly printed one.^{33–39} Such a configuration leaves flexible space for EP state tuning, ensures effective excitation of multipolar modes, and enhances the perturbation strength of target particles (see Sec. S3 in the [Supplementary Material](#) for detailed explanations). The 2.82 mm-wide microstrip line overlaps with the resonator by $d_w = 2$ mm along the y direction. The specific dimensions of the designed resonator are $R = 40$ mm (outer radius), $r = 20$ mm (inner radius), $a = 0.5d$ (periodicity), $t = 0.5$ mm (thickness), and $N = 60$ (number of grooves). To facilitate the introduction of Rayleigh scattering particles and enhance the coupling between the resonator and the scatterers, a metal disk with a radius of $R_d = r = 20$ mm and a thickness of $h_d = 2.5$ mm is fabricated, integrated with the resonator, and positioned between the spoof plasmonic resonator and the substrate. The radii of the scatterers are denoted by r_1 and r_2 , respectively, and their relative azimuthal angle is α with the same thickness of 2 mm. In addition, the feeding line and the ground plane are both $35 \mu\text{m}$ thick, while the F4B dielectric substrate has a thickness $h_s = 0.93$ mm, relative permittivity $\varepsilon_r = 2.2$, loss tangent $\tan \delta = 0.003$, and side length $l_s = 120$ mm.

For the simulations conducted using the commercial software CST Microwave Studio, we set the boundary conditions in the x , y , and z directions as open boundaries. In addition, we supplement these boundaries with a 30 mm-thick air layer in each direction, corresponding to one-quarter wavelength at the center frequency of the simulation bandwidth. Figure 2(d) shows the fabricated spoof plasmonic resonator and setup of the measurement. The transmission spectra of the DP sensor in the absence of external perturbation are shown in Fig. 2(e), which are captured through numerical simulations and measurements. Excellent agreements between the simulated and measured curves demonstrate that a series of plasmonic resonances are excited, which are denoted by nine dips from M_1 to M_9 .

3 Results and Discussion

3.1 Fabrication and Measurement

To experimentally demonstrate the tunability and reconfigurability of the EP spoof plasmonic sensor, we fabricated an aluminum-made resonator prototype and an F4B dielectric substrate using printed circuit board technologies, as shown in Fig. 2(d). The dimensions of the manufactured sensor are identical to those designed in Sec. 2.2. In the measurement, both ends of the microstrip line were connected with the Keysight N9927A vector network analyzer by SMA adaptors to measure the transmission and reflection spectra. To realize second-order EPs for each mode, we introduced a pair of deep-subwavelength Rayleigh scatterers into the evanescent-field regime of the spoof plasmonic resonator by carefully tailoring their radial positions and relative azimuthal angles. Compared with the DP, additional losses introduced by two scatterers not only broaden the linewidth of a specific resonance with enlarged frequency separation when working at the EP but also result in a reduction of the Q -factors of the system to a certain extent. To investigate the performance of this novel sensor, a copper particle was set as the target particle near the resonator and the relative azimuthal angle was set as $\alpha_3 = \pi$ with the same thickness as the scatterers

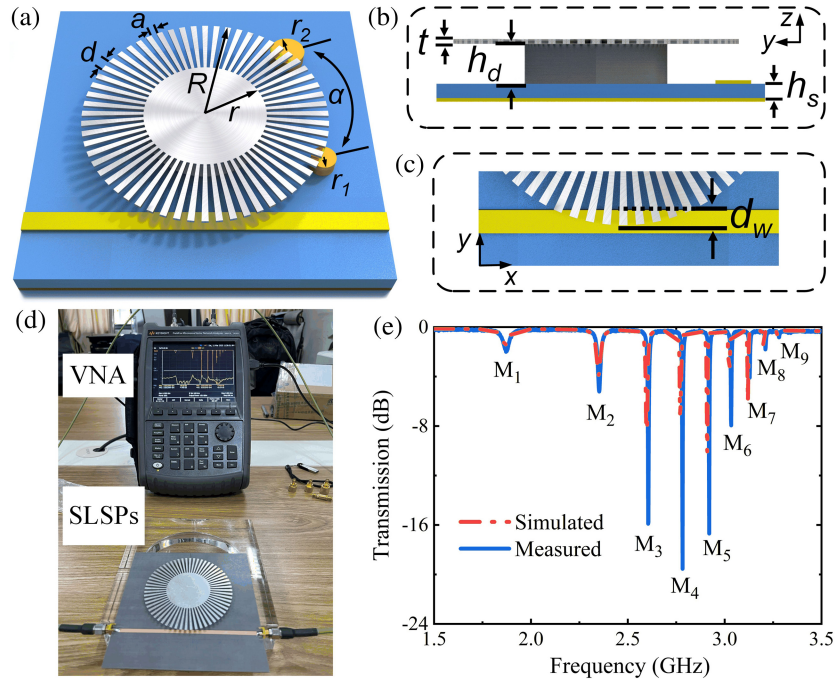


Fig. 2 (a)–(c) Schematic drawing of the proposed reconfigurable EP sensor based on spoof plasmonic resonator. (d) Experimental measurement setup based on a spoof LSP resonator. (e) Comparison of transmission parameters of DP spoof plasmonic sensors between the simulated and measured results. Nine plasmonic modes are collectively excited, starting from the fundamental mode, and the simulation results exhibit excellent agreement with the experimental observations (Video 1, MP4, 14.9 MB [URL: <https://doi.org/10.1117/1.APN.3.5.056004.s1>]).

mentioned earlier. In addition, these particles are fabricated from high-purity copper plates using precision laser cutting techniques.

3.2 Experimental Results

In the proposed spoof plasmonic EP sensing system, we experimentally implement five distinct EPs at the sextu-, octu-, deca-, dodeca-, and fourteen-pole modes (from M_3 to M_7), respectively, with their resonance frequencies of 2.564, 2.765, 2.901, 3, and 3.11 GHz. To achieve EPs at each plasmonic mode, we set the first scatterer at an appropriate position (such as $\alpha_1 = 0$, below the right periphery of the resonator). Then, the second scatterer was deposited near the rim of the spoof plasmonic resonator. By adjusting the azimuthal position of the second scatterer carefully, the corresponding resonance modes degenerate in the transmission spectrum, demonstrating that the sensor is close to the EP state. However, the radial and azimuthal positions of both scatterers need to be slightly tuned until the reflection coefficients of different input ports reach the maximum deviation. One single broadened resonance dip and fully asymmetric reflection coefficients indicate the occurrence of EPs in the measurement, which correspond to non-Hermitian degeneracies of the resonance modes. Specifically, for five consecutive resonance modes (M_3 to M_7), the dimensions and positions of the corresponding pair of scatterers are listed in Table 1 and depicted in Figs. 3(a)–3(e). The details of particles, along with a comparison of S -parameters between the measured and simulated reconfigurable EPs, are discussed in Sec. S4 in the [Supplementary Material](#).

As shown in Figs. 3(f)–3(j), the left panels show the resonance dip of the DP and EP sensors in the absence of the target particle. The introduction of two external scatterers leads to extra backscattering, resulting in a significant increase in the linewidth of the resonance dip. Meanwhile, the single target particle placed near the resonator ($\alpha_3 = \pi$) lifts the degeneracy of corresponding eigenmodes, and the frequency splitting of EP sensors is noticeably greater than that of DP sensors. Furthermore, the sensitivity enhancements highlighted by black dashed lines are quite evident [see the right panels in Figs. 3(f)–3(j)]. As the essence of EPs, the scatterers utilized to establish EPs bring in extra losses, i.e., excess asymmetric backscattering between the counterpropagating waves. Therefore, when the signal is injected from one end of the microstrip line (such

Table 1 Scatterer dimensions and positions of the reconfigurable EP sensors.

Mode	Frequency (GHz)	Scatterers (r_1, r_2) (mm)	Relative Azimuthal Angle α_{mj} (deg)
M_3	2.564	(3, 3.5)	23
M_4	2.765	(2.25, 2.5)	61
M_5	2.901	(2, 2.25)	50
M_6	3	(3, 3.5)	37
M_7	3.11	(2, 2.5)	34

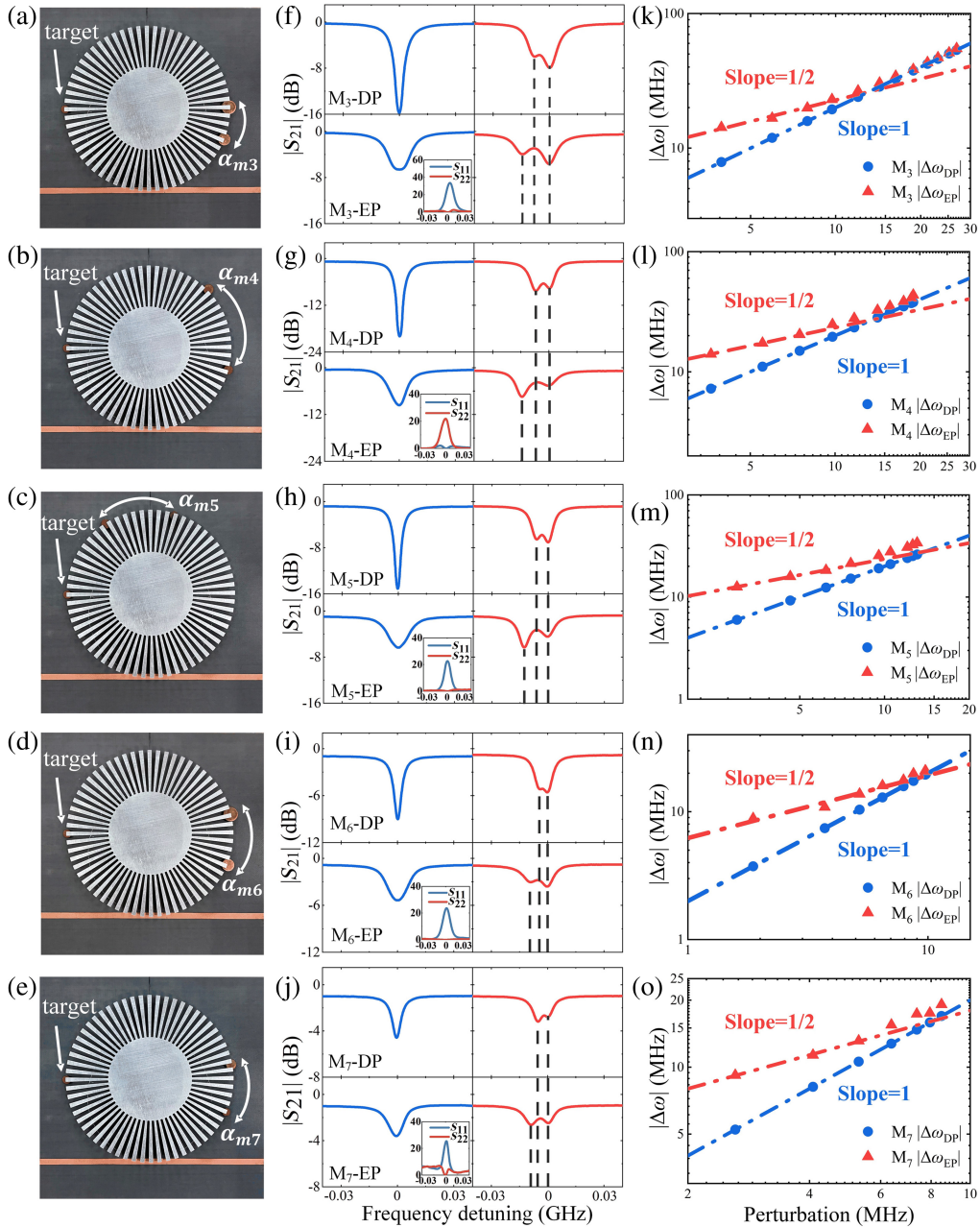


Fig. 3 Schematic diagrams of the reconfigurable EP sensing systems on the single-spoof plasmonic resonator with the relative azimuthal angle between scatterers: (a) $\alpha_{m3} = 23$ deg, (b) $\alpha_{m4} = 61$ deg, (c) $\alpha_{m5} = 50$ deg, (d) $\alpha_{m6} = 37$ deg, and (e) $\alpha_{m7} = 34$ deg. Target particles are positioned at the same location ($\alpha_3 = \pi$). (f)–(j) The measured transmission spectra of DP (top panels) and EP (bottom panels) sensors before (blue curves in the left panels) and after (red curves in the right panels) introducing a deep-subwavelength metal target into the vicinity of the spoof plasmonic resonator. Black vertical dashed lines in the right panels highlight the enhancements of sensitivity. The insets depict fully asymmetric reflection coefficients, indicating the occurrences of EPs. The abscissa axes of the inset figures represent frequency detuning (in gigahertz), while the ordinate axes represent the normalized reflection coefficients (in a.u., arbitrary units). (k)–(o) Relationships between the frequency splitting of DP (blue) and EP (red) sensors and the perturbation strength on logarithmic scales. The frequency-splitting responses in EP sensors demonstrate the slope of 1/2, which is proportional to $\varepsilon^{1/2}$ and consistent with the prediction of Eq. (2).

as port 1), the reflection spectrum exhibits a strong peak at the resonance frequency. On the contrary, the reflection almost disappears while injecting from the other port (such as port 2), as depicted in the insets of Figs. 3(f)–3(j). It is worth noting that the noticeable deviation of the reflection coefficients generated by different port inputs represents an important criterion for determining reconfigurable EPs in the real-time spoof plasmonic sensing system.

Figures 3(k)–3(o) depict the relation between the frequency splitting of DP and EP sensors and the perturbation strength on a logarithmic scale. The relation in DP sensors is validated by the slope of 1, confirming that conventional sensors are linearly correlated with the perturbation strength. Meanwhile, when the perturbation is adequately small ($|A_j^{(2)}| \gg |\epsilon|$), EP sensors attract the frequency-splitting responses that demonstrate the slope of 1/2, which are proportional to $\epsilon^{1/2}$ and consistent with the prediction of Eq. (2). With respect to sensors operating at EPs, the frequency splitting produced by larger target particles gradually increases beyond the slope of 1/2 and even becomes comparable to that of DP sensors. This consequence arises from the fact that when the measured target is relatively large ($|A_j^{(2)}|$ is approximate to $|\epsilon|$), Eq. (1) cannot be simplified to Eq. (2).

The histograms in Figs. 4(a)–4(e) illustrate the variations and comparisons of the frequency-splitting responses in DP and EP sensors when targets with different diameters are deposited near the resonator (see Sec. S5 in the [Supplementary Material](#) for detailed measured spectra). Note that the measurements were

conducted 3 times under identical conditions, and the mean values of the three samples were used to represent the measured data. Remarkably, the light blue regions reveal that sensors working at EPs are capable of resolving smaller particles compared with DP sensors, validating their enhanced interactions with target particles. In addition, each EP sensor working at the corresponding plasmonic mode possesses a certain detectable range for targets of different dimensions. Experimental results indicate that modes of lower orders are capable of detecting larger particles. This is because lower frequencies correspond to longer wavelengths, which makes the resonator more suitable for detecting larger targets. In particular, the EP sensor operating at sextupole mode (M_3) manifests the widest range of detectable particle sizes. The minimum target with the dimension of 0.001λ can be resolved in the 14-pole mode (M_7). Furthermore, the prominent advantage of the proposed tunable and reconfigurable EP sensors is that they are capable of detecting particles much smaller than those detected by DP sensors across all five operating plasmonic modes. As the mode order increases, the minimum resolvable target size diminishes accordingly. It is demonstrated that the EP sensor working at M_7 can identify a single target with a diameter of 0.1 mm, equivalent to the electrical length of 0.001λ (wavelength of the 14-pole mode).

The sensitivity enhancements $|\Delta\omega_{EP}/\Delta\omega_{DP}|$, which refer to the amplifications of frequency splitting in EP sensors compared to DP sensors, are illustrated in the insets of Figs. 4(a)–4(e). The dots in various colors represent the correlation between $|\Delta\omega_{EP}/\Delta\omega_{DP}|$ and the perturbation strength ϵ acquired from the

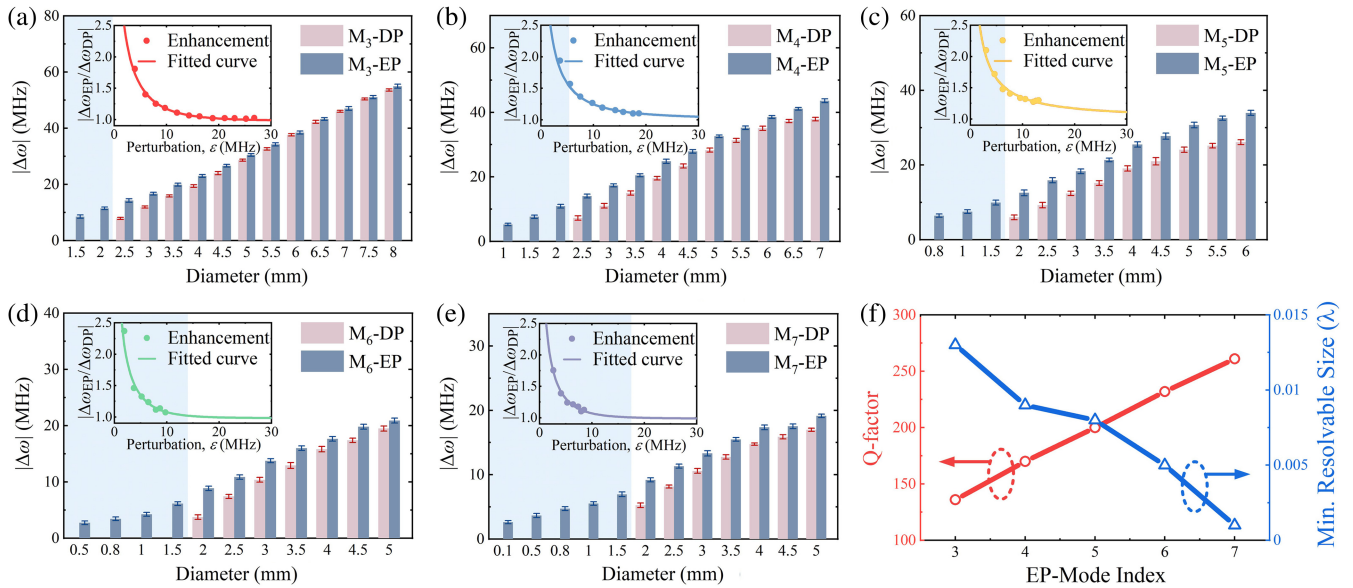


Fig. 4 Histograms depicting the variations and comparative analysis of the measured frequency-splitting responses (mean values of the experimental results repeated 3 times) induced by the DP and EP sensors with various targets at (a) sextu-, (b) octu-, (c) deca-, (d) dodeca-, and (e) fourteen-pole modes. The whiskers represent the range of results from three measurements. The insets illustrate sensitivity enhancements that refer to the ratio between the frequency splitting of EP sensors and that of DP sensors. The dots in various colors represent the correlation between $|\Delta\omega_{EP}/\Delta\omega_{DP}|$ and the perturbation strength ϵ , which conform well to the fitted lines derived from Eq. (1). To be specific, the values of $A_j^{(2)} e^{i2m_j\alpha}$ ($j = 3, 4, 5, 6, 7$) in Eq. (1) of the five proposed reconfigurable EPs are as follows: $-3 + 11.8i$, $1.2 - 10.8i$, $6.3 - 7.5i$, $-2.2 + 8.6i$, and $-1.6 + 7.8i$, respectively. (f) Variation of the Q -factors and minimum resolvable sizes with the EP-mode index of the proposed reconfigurable EP sensors (Video 2, MP4, 12.6 MB [URL: <https://doi.org/10.1117/1.APN.3.5.056004.s2>]).

Table 2 Comparison of the experimental results between the proposed reconfigurable EP-based spoof plasmonic sensor and previous works.

Reference	Resonator	Mode	Frequency (GHz)	Q -factor	Minimum Resolvable Diameter	Target Thickness (mm)	$\Delta\omega_{EP}/\Delta\omega_0$ ($\times 10^{-3}$)
24	Microtoroid cavity	—	193,500	3×10^7	0.258λ	4×10^{-4}	1.6×10^{-4}
39	Spoof LSPs	M_1	2.604	129	0.004λ	0.035	6.3
40	Spoof LSPs	M_3	6.185	200	0.012λ	0.035	1.3
41	Spoof LSPs	M_6	5.595	94	0.019λ	0.018	8.1
This work	Reconfigurable EP-based spoof LSPs	M_3	2.564	136	0.013λ	2	3.3
		M_4	2.765	170	0.009λ	2	1.9
		M_5	2.901	200	0.008λ	2	2.2
		M_6	3	232	0.005λ	2	0.9
		M_7	3.11	261	0.001λ	2	0.8

measurement, which conforms well to the fitted lines derived from Eq. (1). From the predicted fitting curves, we can estimate that when the target particle is small, the enhancements of all five EPs tend to be similar. However, the EP sensor working at the decapole mode (M_5) exhibits the most enhanced sensitivity across the whole dimension range of targets. In particular, the dodecapole mode (M_6) demonstrates the optimal sensitivity enhancement by the factor of 2.4 (frequency splitting with 3.74 MHz in the DP sensor enhanced to 8.86 MHz in the EP sensor). More details regarding the sensitivity enhancement are described in Sec. S6 in the [Supplementary Material](#). Notably, the fluctuations between the experimental results and the fitting curves of the formula originate from tiny deviations generated by the manufacturing process and the instability of ambient temperature. In addition, the Q -factors of the reconfigurable EP sensors are scrupulously calculated by analyzing the transmission spectra, resulting in values of 136, 170, 200, 232, and 261 at each resonance mode, respectively. As depicted in Fig. 4(f), when the mode order increases, the corresponding Q -factor also exhibits an increase, and the minimum resolvable size of targets becomes smaller. Compared with previous EP-based WGM sensors in Table 2, our work achieves an unprecedented improvement in tunability and reconfigurability of EP sensing and extends the minimum resolvable limit of targets with high Q -values concurrently in a purely passive EP system.

4 Conclusion

In summary, we have proposed an experimental flexibly reconfigurable multimode EP sensor that capitalizes on the spoof plasmonic system coupled to two adjustable Rayleigh scatterers at microwave frequencies. Owing to strong field confinement at the boundaries of resonators, this novel sensor realizes five consecutive EPs in a broad range of frequencies and exhibits more than twofold sensitivity enhancement for the deep-subwavelength target detection. The range of detectable particle sizes is also widened. Meanwhile, our proposed sensors have two additional advantages: first, the tunability and flexibility of this system make it easy to realize EPs even in the presence of fabrication errors; second, compared with traditional ways based on frequency shift, the sensitivity of our proposed sensors depends on the frequency splitting; thus our system is highly robust.^{20,22}

Last but not least, our scheme not only can be transferred to other frequency bands (e.g., terahertz/infrared frequencies), as introduced in Sec. S7 in the [Supplementary Material](#), but also inspire the future design of novel applications such as multi-channel asymmetric transportation,¹³ reconfigurable topological lasers,¹⁴ and intelligent phononic metamaterials.⁴²

Code and Data Availability

The data that support the findings of this study are provided in the [Supplementary Material](#) and are available from the corresponding author upon request.

Acknowledgments

This work was supported by the National Natural Science Foundation of China (Grant Nos. 61871215, 61771238, and 61701246), the National Key Research and Development Program of China (Grant No. 2022YFA1404903), the Fund of Qing Lan Project of Jiangsu Province (Grant No. 1004-YQR22031), the Six Talent Peaks Project in Jiangsu Province (Grant No. 2018-GDZB-009), the Fund of Prospective Layout of Scientific Research for NUAA (Nanjing University of Aeronautics and Astronautics) (Grant Nos. 1004-ILA22002 and 1004-ILA22068), the Research and Practice Innovation Program of Nanjing University of Aeronautics and Astronautics (Grant No. xcjxh20210408), the Postgraduate Research & Practice Innovation Program of Jiangsu Province (Grant No. KYCX22_0364), the Fundamental Research Funds for the Central Universities, NUAA (Grant No. NS2023022), the Nanjing University of Aeronautics and Astronautics Start-up Grant (Grant No. 1004-YQR23031), the Distinguished Professor Fund of Jiangsu Province (Grant No. 1004-YQR24010), Fundamental Research Funds for the Central Universities, NUAA (No. NE2024007), and the Singapore National Research Foundation Competitive Research Program (NRF-CRP22-2019-0006).

References

1. C. Dembowski et al., "Experimental observation of the topological structure of exceptional points," *Phys. Rev. Lett.* **86**(5), 787–790 (2001).

2. B. Peng et al., "Loss-induced suppression and revival of lasing," *Science* **346**(6207), 328–332 (2014).
3. T. Gao et al., "Observation of non-Hermitian degeneracies in a chaotic exciton-polariton billiard," *Nature* **526**(7574), 554–558 (2015).
4. D. Liu et al., "Simultaneous manipulation of line-gap and point-gap topologies in non-Hermitian lattices," *Laser Photonics Rev.* **17**(4), 2200371 (2023).
5. S. Malzard, C. Poli, and H. Schomerus, "Topologically protected defect states in open photonic systems with non-Hermitian charge-conjugation and parity-time symmetry," *Phys. Rev. Lett.* **115**(20), 200402 (2015).
6. J. Doppler et al., "Dynamically encircling an exceptional point for asymmetric mode switching," *Nature* **537**(7618), 76–79 (2016).
7. Y. D. Chong, G. Li, and A. D. Stone, "PT-symmetry breaking and laser-absorber modes in optical scattering systems," *Phys. Rev. Lett.* **106**(9), 093902 (2011).
8. C. Wang et al., "Coherent perfect absorption at an exceptional point," *Science* **373**(6560), 1261–1265 (2021).
9. M. P. Hokmabadi et al., "Non-Hermitian ring laser gyroscopes with enhanced Sagnac sensitivity," *Nature* **576**(7785), 70–74 (2019).
10. Y. Choi et al., "Extremely broadband, on-chip optical nonreciprocity enabled by mimicking nonlinear anti-adiabatic quantum jumps near exceptional points," *Nat. Commun.* **8**(1), 14154 (2017).
11. B. Peng et al., "Chiral modes and directional lasing at exceptional points," *Proc. Natl. Acad. Sci. U. S. A.* **113**(25), 6845–6850 (2016).
12. H. Zhao et al., "Non-Hermitian topological light steering," *Science* **365**(6458), 1163–1166 (2019).
13. A. Li et al., "Exceptional points and non-Hermitian photonics at the nanoscale," *Nat. Nanotechnol.* **18**(7), 706–720 (2023).
14. A. Schumer et al., "Topological modes in a laser cavity through exceptional state transfer," *Science* **375**(6583), 884–888 (2022).
15. M.-A. Miri and A. Alù, "Exceptional points in optics and photonics," *Science* **363**(6422), eaar7709 (2019).
16. J. Wiersig, "Structure of whispering-gallery modes in optical microdisks perturbed by nanoparticles," *Phys. Rev. A* **84**(6), 063828 (2011).
17. L. Shao et al., "Detection of single nanoparticles and lentiviruses using microcavity resonance broadening," *Adv. Mater.* **25**(39), 5616–5620 (2013).
18. W. Chen et al., "Parity-time-symmetric whispering-gallery mode nanoparticle sensor," *Photonics Res.* **6**(5), A23–A30 (2018).
19. G.-Q. Qin et al., "Experimental realization of sensitivity enhancement and suppression with exceptional surfaces," *Laser Photonics Rev.* **15**(5), 2000569 (2021).
20. J. Zhu et al., "On-chip single nanoparticle detection and sizing by mode splitting in an ultrahigh-Q microresonator," *Nat. Photon.* **4**(1), 46–49 (2009).
21. D. Liu, H. Hu, and J. Zhang, "Edge states in coupled non-Hermitian resonators," *Opt. Lett.* **48**(11), 2869–2872 (2023).
22. J. Wiersig, "Enhancing the sensitivity of frequency and energy splitting detection by using exceptional points: application to microcavity sensors for single-particle detection," *Phys. Rev. Lett.* **112**(20), 203901 (2014).
23. J. Wiersig, "Sensors operating at exceptional points: general theory," *Phys. Rev. A* **93**(3), 033809 (2016).
24. W. Chen et al., "Exceptional points enhance sensing in an optical microcavity," *Nature* **548**(7666), 192–196 (2017).
25. B. Arash, J. W. Jiang, and T. Rabczuk, "A review on nanomechanical resonators and their applications in sensors and molecular transportation," *Appl. Phys. Rev.* **2**(2), 021301 (2015).
26. X. Zhang et al., "Spoof localized surface plasmons for sensing applications," *Adv. Mater. Technol.* **6**(4), 2000863 (2021).
27. J. B. Pendry, L. Martín-Moreno, and F. J. García-Vidal, "Mimicking surface plasmons with structured surfaces," *Science* **305**(5685), 847–848 (2004).
28. Z. Li et al., "Mimicking localized surface plasmons with structural dispersion," *Adv. Opt. Mater.* **7**(10), 1900118 (2019).
29. Z. Li et al., "Multi-band localized spoof plasmons with texturing closed surfaces," *Appl. Phys. Lett.* **104**(10), 101603 (2014).
30. Z. Gao et al., "Localized spoof surface plasmons in textured open metal surfaces," *Opt. Lett.* **41**(10), 2181–2184 (2016).
31. F. J. García-Vidal et al., "Spoof surface plasmon photonics," *Rev. Mod. Phys.* **94**(2), 025004 (2022).
32. A. Pors et al., "Localized spoof plasmons arise while texturing closed surfaces," *Phys. Rev. Lett.* **108**(22), 223905 (2012).
33. X. Shen and T. J. Cui, "Ultrathin plasmonic metamaterial for spoof localized surface plasmons," *Laser Photonics Rev.* **8**(1), 137–145 (2014).
34. X. Zhang and T. J. Cui, "Deep-subwavelength and high-Q trapped mode induced by symmetry-broken in toroidal plasmonic resonator," *IEEE Trans. Antennas Propag.* **69**(4), 2122–2129 (2021).
35. X. Zhang et al., "Wide-bandpass filtering due to multipole resonances of spoof localized surface plasmons," *Ann. Phys.* **530**(11), 1800207 (2018).
36. Z. Liao et al., "High-order localized spoof surface plasmon resonances and experimental verifications," *Sci. Rep.* **5**(1), 9590 (2015).
37. Q. Zhou et al., "Plasmonic bound states in the continuum in compact nanostructures," *Adv. Opt. Mater.* **10**(24), 2201590 (2022).
38. H. Y. Jeong et al., "Electrical addressing of exceptional points in compact plasmonic structures," *Nanophotonics* **12**(11), 2029–2039 (2023).
39. T. S. Bai et al., "Exceptional point in a microwave plasmonic dipole resonator for sub-microliter solution sensing," *Adv. Funct. Mater.* **34**(13), 2312170 (2024).
40. Z. Liao et al., "Microwave plasmonic exceptional points for enhanced sensing," *Laser Photonics Rev.* **17**(11), 2300276 (2023).
41. J. Chen et al., "Coherent-resonance enhancement of sensing at the exceptional points," *Adv. Opt. Mater.* **12**(10), 2302268 (2024).
42. Y. Jin et al., "Intelligent on-demand design of phononic metamaterials," *Nanophotonics* **11**(3), 439–460 (2022).

Yaoran Zhang received his BS degree in electronic information science and technology from the Nanjing University of Aeronautics and Astronautics (NUAA), Nanjing, China, in 2018, where he is currently pursuing his PhD in information and communication engineering. His current research interests include plasmonic metamaterials, spoof LSP-based EP sensors, and parity-time symmetry.

Hao Hu has been a professor in the College of Electronic and Information Engineering of NUAA since 2023. His research interests include metamaterials, photonic crystals, spatial nonlocality, Cherenkov radiation, nonreciprocal optics, and scattering optics. He is also interested in topological physics and spatiotemporal metamaterials.

Francisco José García-Vidal is a full professor at the Universidad Autónoma de Madrid, Madrid, Spain. His current research interests include surface-enhanced Raman scattering and highly absorptive metamaterials, spoof surface plasmons, light waveguiding, and quantum plasmonics. He is also interested in near-field radiative heat transfer and polaritonic chemistry and materials science.

Jingjing Zhang received her PhD from the Zhejiang University, Hangzhou, China, in 2009. She has been an H. C. Ørsted Post-Doctoral Researcher Fellow and an assistant professor at the Technical University of Denmark, Lyngby, Denmark, a Newton International Fellow at the King's College London, London, United Kingdom, and a senior research fellow at the Nanyang Technological University, Singapore. She is currently a professor at the State Key Laboratory of Millimeter Waves, Southeast University, Nanjing, China. Her research interests include metamaterials, nanoplasmonics, and designer surface plasmons.

Liangliang Liu has been an associate professor in the College of Electronic and Information Engineering of NUAA since 2020. His current research interests include microwave and millimeter-wave devices and antennas technology, frequency-selective surfaces, spoof surface plasmons, effective surface plasmons, and coding metasurfaces.

Yu Luo is currently a professor at the College of Electronic and Information Engineering of NUAA. Prior to joining NUAA, he was an associate professor and deputy director of the Centre for Optoelectronics and Biophotonics at the School of Electrical and Electronic Engineering of Nanyang Technological University. He works on a wide range of topics within the realm of metamaterials and plasmonics, ranging

from the design of invisibility cloaks and plasmonic light-harvesting devices to the study of nonlocal and quantum phenomena in mesoscopic plasmonic systems.

Zhuo Li is currently a full professor at the College of Electronic and Information Engineering of NUAA, Nanjing, China. His current research interests include plasmonic metamaterials, MHz-through-THz technologies and transceivers for wireless sensors and biomedical applications, electromagnetic compatibility in avionics systems, and auto-electrical systems. He is also interested in the modeling and design of microwave and terahertz photonic circuits and systems.